Hindawi
Geofluids
Volume 2019, Article ID 3016563, 17 pages
https://doi.org/10.1155/2019/3016563

*Research Article*

# Determination of the Hydration Damage Instability Period in a Shale Borehole Wall and Its Application to a Fuling Shale Gas Reservoir in China

**Haicheng She**,[1] **Zaiqiang Hu**,[1] **Zhan Qu**,[2] **Yao Zhang**,[1] **and Hu Guo**[3]

[1]*School of Civil Engineering and Architecture, Xi'an University of Technology, Xi'an, 710048 Shaanxi, China*
[2]*School of Petroleum Engineering, Xi'an Shiyou University, Xi'an, 710065 Shaanxi, China*
[3]*School of Petroleum Engineering and Environment Engineering, Yan'an University, Yan'an, 716000 Shaanxi, China*

Correspondence should be addressed to Zaiqiang Hu; huzq@xaut.edu.cn and Hu Guo; truetutors@126.com

Received 10 August 2018; Revised 26 December 2018; Accepted 4 March 2019; Published 2 June 2019

Academic Editor: Reza Rezaee



In reviewing Chinese shale gas reserves and national policies regarding shale gas exploitation, shale gas will be of critical importance in providing clean natural gas to China. However, compared to those in the United States, the cost of shale gas extraction and the complex problems encountered in more complex and deep drilling in China are key technologies that need to be overcome. Shale wellbore wall instability is a complex problem that often occurs during drilling. During the process of drilling in shale, the complex stress and fluid-structure interactions result in the wall rock generating a strong hydration diffusion and swelling effect, which alters the stress distribution in the rock wall and deteriorates the mechanical parameters of the rock. This results in instability damage of the shale wellbore wall. In this study, the stratigraphic stress characteristics of the Fuling Shale Gas Field were initially predicted, and the shale sample phase composition and development of bedding and microcracks were analyzed using X-ray diffraction and scanning electronic microscopy. The main driving potential difference function between the drilling fluid and shale was analyzed, and a radial adsorption diffusion model of the shale plane was established. Through a laboratory study, the space time change law of the water diffusion of the shale rock was assessed as well as the rock damage evolutionary law of the elastic modulus and compressive strength with water content. Then, combined with the shale hydration stress and strength deformation theory, a damage evolutionary equation for shale with water was derived, and the shale damage evolutionary limit equation and the method of determining the collapse cycle were established. Finally, the method was applied to the Fuling Shale Gas Field, the largest shale gas field in China, and a shale wellbore collapse cycle of approximately seven days in the field was obtained. The severity of economic loss resulting from wellbore wall instability was also determined. This study provides insight and guidance for reducing the costs of shale gas reservoir well drilling and efficient development.

## 1. Introduction

The revolution of shale gas in the United States of America (USA) is changing the energy structure of the world [1]. The shale oil and shale gas revolution in the USA has significantly changed the global energy structure and made the USA the largest oil and gas producer in 2018. The shale gas production in China during recent years has been far less than that in the USA. Although China is the third most productive country commercially producing shale gas after the USA and Canada, the cost in China is much higher than that in the USA [2], as shown in Figure 1. Several reasons, such as shale gas policy [3], technology level [4], and geological factors [5, 6], account for this discrepancy. The greatest cause or result is the comprehensive cost difference in exploiting shale gas. The latest cost of shale gas in the USA and China is worth noting. During 2015, the drilling and production costs of a horizontal shale gas well in the United States were approximately US$ 2.50–5.50 million (RMB 16–35 million) [7], while in China, it was typically higher (approximately RMB 65–80 million for a horizontal well) during the initial development stage. The high cost of shale gas makes China

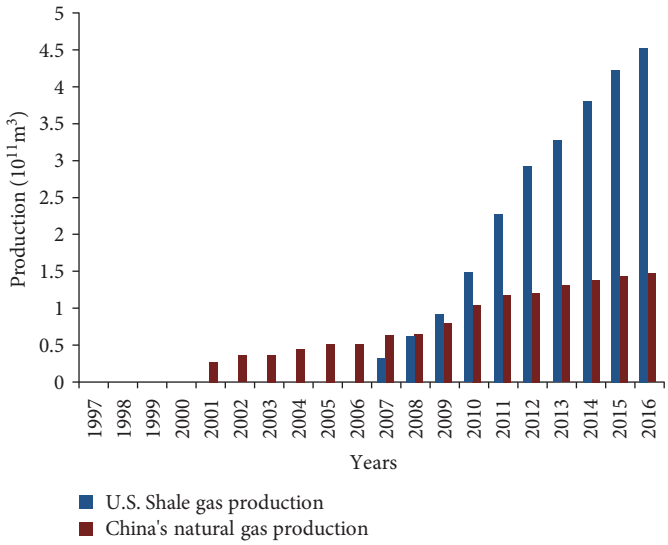


Figure 1: Shale gas production in China and the USA.

less competitive and prevents the country's shale gas industry from achieving the same success as that in the USA. However, the shale gas reserves [8] in China are predicted to be higher than those of the USA, as shown in Figure 2. As seen in Figure 3, shale gas reserves [9] are mainly distributed in the Sichuan Basin, Jianghan Basin, and Guizhou-Guangxi shale gas area in the eastern Yangtze region. In terms of the shale gas cost composition, the major costs are well drilling and multistage fractures. Although the total cost of well drilling can be reduced by increasing the number of wells, reducing the cost of a single well is of vital importance. Any factors that affect shale gas well drilling, such as wellbore wall stability and well completion quality, have a direct influence on the shale gas cost.

During the process of oil and gas drilling, complex issues such as collapse, hole shrinkage, and sticking, which are caused by the instability of borehole walls in the downhole, present serious problems in the drilling engineering field. According to a conservative estimate, these problems result in more than $1 billion USD/year in economic losses [10]. In the Changqing, Tarim, and Turpan Hami oil and gas fields of China, the shales comprise over 75% of the drilled formations and present over 90% of the wellbore instability problems. Thus, wellbore stability is important for wells in both conventional and unconventional reservoirs. During the process of shale gas reservoir exploration and development, shale is not only the reservoir body of shale oil and gas resources but also the geological body of wellbore instability and underground complications in the drilling process. How to safely, quickly, efficiently, and cost-effectively drill regular and longer horizontal wells is a core technology and a major technical difficulty of shale gas development.

At present, more attention has been paid to the study of well instability, and numerous achievements have been made. Water-based muds provide an attractive alternative, but they have shown poor shale drilling performance [11]. The extent to which shale is disturbed because of well excavation can be assessed using a suitable analysis of the forces

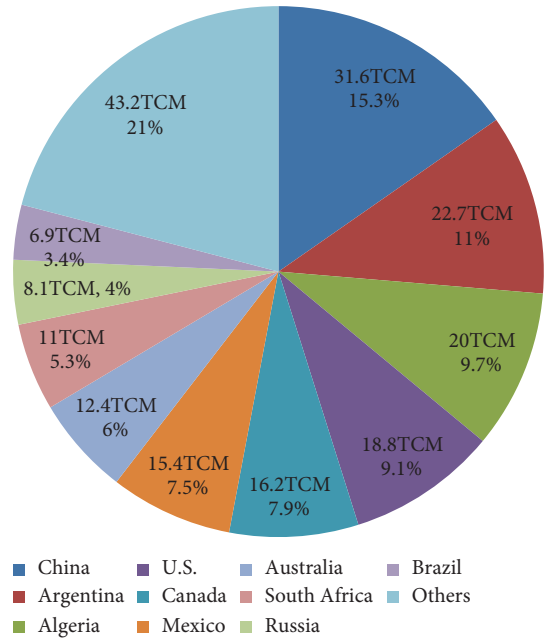


Figure 2: Top 10 countries with technically recoverable shale gas resources [8].

imposed on the rock by the disequilibria resulting from the drilling action [12, 13]. The chemomechanical processes causing shale deterioration and borehole instability while drilling have been studied by a number of investigators. Although some significant progress has been made [14–16], an adequate tool for analyzing shale deformation while drilling is not presently available. The mechanical and chemical effects on shale stability have been organically combined using a combination of rock mechanics and seepage theory, and moreover, the effects of various physical and chemical reactions between the drilling fluid and shale formation

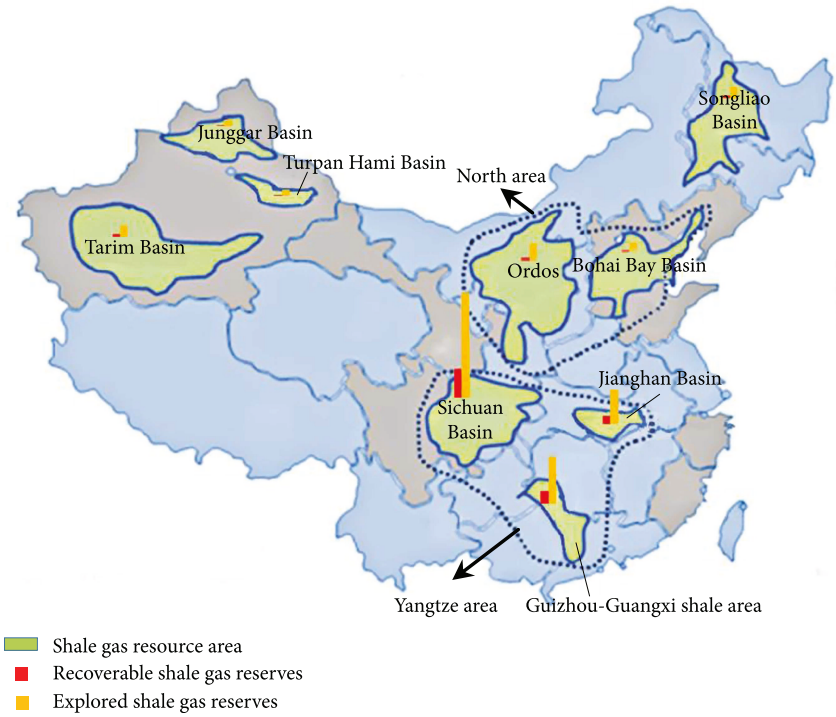


Distribution of shale gas resources in China

| Basins | ESGR $10^{12}m^3$ | RSGR $10^{12}m^3$ |
|---|---|---|
| Sichuan Basin | 76.43 | 21.17 |
| Jianghan Basin | 18.76 | 5.05 |
| Guizhou-Guangxi shale area | 13.61 | 3.37 |
| Ordos | 7.17 | 1.82 |
| Songliao Basin | 4.74 | 1.08 |
| Bohai Bay Basin | 4.33 | 1.07 |
| Tarim Basin | 4.42 | 1.32 |
| Junggar Basin | 2.64 | 0.57 |
| Turpan Hami Basin | 2.32 | 0.55 |

ESGR is explored shale gas reserves
RSGR is recoverable shale gas

Figure 3: Shale reserves of the main basins of China.

(underground fluid) on the stability of the shale borehole walls have been comprehensively investigated [17–20]. In addition, research on shale chemomechanical stability coupling the two aspects of experiment and theory has also been analyzed [21–25]. Micromeasurement techniques have been used to analyze shale characteristics of mineral composition, microcracks, and bedding [26, 27]. Some scholars have proposed and studied the influence of weak plane structures such as bedding and crack planes on the stability of the borehole wall [28–31] and have established the strength criterion of a single weak plane and multiple weak planes in the surrounding rock of shale wellbores [32–36]. In addition, some scholars have used X-ray CT, SEM, and NMR micromeasurement techniques to identify hydration shale damage characteristics and study damage evolution laws, proposing different constitutive damage models [37–39]. It is worth emphasizing that some scholars and engineers have applied micro-/nanotechnology to the study of wellbore instability and have formulated different nanoparticle drilling fluids to improve fluid thermal stability; provide better lubricity, hole cleaning, and wellbore stability; and mitigate hydrate formation within the fluid circulation system. Many types of these nanoparticles, such as silica nanocomposite, clay nanocomposite, palygorskite, sepiolite, attapulgite, and others, have been formulated [40–44]. With the extension of drilling to deeper layers, the high temperature and high pressure of the formation have attracted the attention of many scholars. The formation temperature affects not only the operation of the drilling equipment and the performance of the drilling fluid but also the temperature difference between the formation and the drilling fluid, which will affect the stability of the shale wall [45–47].

However, to date, there are few references reported using the combination of damage mechanics and seepage mechanics on the basis of chemomechanical coupling to study the hydration damage of shale borehole instability during oil and gas drilling. In this study, the specific research work is summarized as follows: First, the shale components, microstructure, and stratigraphic stress characteristics were analyzed to determine the geological factors of shale damage. Second, the main driving potential difference function between the drilling fluid and shale was analyzed, and the radial adsorption diffusion model of the shale plane was established. Through the rock mechanic parameters (elastic modulus and compressive strength), the law of a damage constitutive model was discussed, and the wellbore damage evolutionary process was shown, e.g., the change in the mechanical parameters of the surrounding rock, damage constitutive model, and strength criterion. Finally, the data were numerically analyzed using theoretical calculation models under real-time conditions to create a model more in line with the actual production situation.

## 2. Fuling Shale Gas Field

According to the existing geological data and a productivity evaluation, the Fuling Shale Gas Field [48] has 2.1 trillion $m^3$ reserves of resources and is the largest shale gas field in China. It is in the southeastern part of the eastern Sichuan fold belt, Wanxian compound, and raises diagonally to the south. The main body of the Jiao Shi dam is a wide-trending anticlinal structure controlled by the Great Luoshan Fault. The main target layers are the Lower Silurian Longmaxi Formation and the Upper Ordovician Wufeng

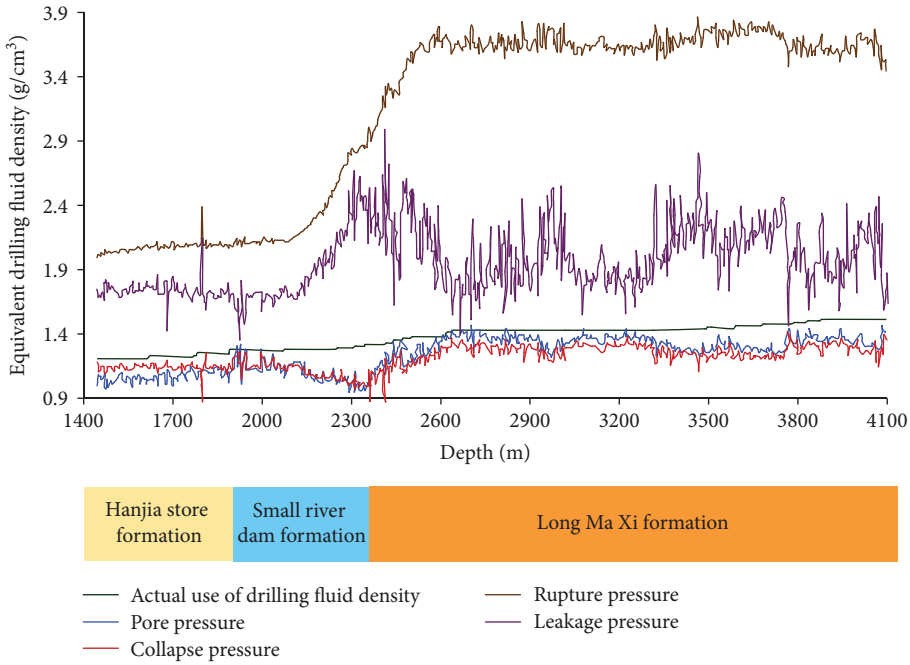


Figure 4: Four pressure prediction curves in the Fuling Shale Gas Field.

Formation. In the Sichuan Basin, the buried depth is greater than 2300 m. During this experiment, rock samples were collected from the Longmaxi Formation, which is a black shale at a vertical depth of 2347.4–2379.5 m. The samples are characterized by dense lithology, fractures and bedding development, a total porosity of 4.22%–6.57%, and a matrix permeability of $0.0023 \times 10^{-3}$ $\mu m^2$–$0.0822 \times 10^{-3}$ $\mu m^2$. The formation temperature gradient is approximately 3.5°C/100 m, and the highest temperature is 80.5°C. Many scholars have used different methods to predict the formation pressure of the Fuling Shale Gas Field. According to rock mechanics and seismic inversion principles, a new method for predicting directional well stability while drilling was proposed. Pore, collapse, rupture, and leakage pressures were established by analyzing the quantitative relationship between seismic data and rock mechanics parameters [49], as shown in Figure 4.

*2.1. Analysis of Rock Mineral Composition.* The mineral composition of the whole rock was analyzed using X-ray diffraction, and the X-ray diffraction distribution curve of the sample was obtained using pseudo-Voigt function fitting and by analyzing the overlapping peaks (Figure 5). The percentage of various phase contents was calculated using the Rietveld method after determining the phase composition of the samples via qualitative and quantitative analyses (Table 1).

The results of the X-ray diffraction analysis show that the clay minerals are mainly mixed-layer illite/smectite and chlorite in the study area, accounting for approximately 54% of the fresh mother rock. Quartz, feldspar, and pyrite are the most important primary minerals, and the content of detrital minerals is approximately 40% of that in the fresh weathered rock, in which the content of quartz is higher. The content of mixed-layer chlorite/smectite and illite is higher than that of chlorite; therefore, mixed-layer chlorite/smectite and illite are the main cause of the deformation due to weak expansion, but the effect is more significant. Because the relative content of quartz and carbonate and clay minerals has a great influence on the physical properties of rocks, their brittleness index [50] can be determined and calculated according to the core mineral analysis as follows:

$$\text{Brittleness index} = \frac{\text{quartz content}}{\text{quartz content} + \text{carbonate content} + \text{clay content}} \times 100\%. \quad (1)$$

As a result, the brittleness of the rock is directly proportional to the quartz content and inversely proportional to the clay content. This brittle hard formation is more likely to result in fractures, which would further likely cause borehole wall damage and instability.

*2.2. Mesostructural Features of Rocks.* The microstructure core was studied using the arrangement and cementation structure of the clay minerals analyzed by scanning the shale core slices from the field. From the results of the scanning electronic microscopy (SEM) experiments as shown in Figures 6(a) and 6(b), intergranular mixed-layer illite/smectite clay, other interstitial materials, and residual hole seams (magnified 4000 times) are apparent. It was found that the microcracks on the rock surface are in a sheet-oriented distribution.

The rock is mainly composed of mixed-layer illite/smectite and illite, which have a certain degree of expansion. The compaction degree of shale is high with the development of horizontal bedding and microfractures in the regional strata.

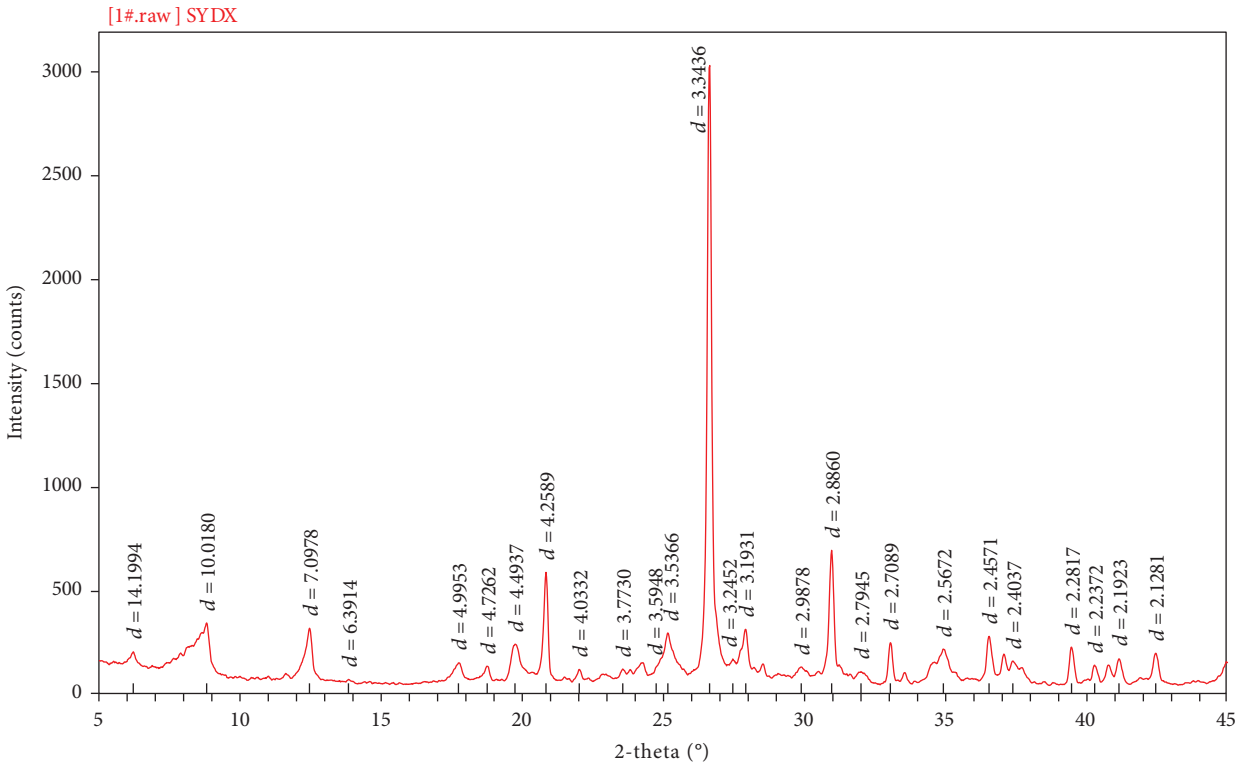


Figure 5: X-ray diffraction energy spectrum of the rock sample.

Table 1: Mineral components of shale samples.

| Minerals | | Quartz | Feldspar | Calcite | Dolomite | Siderite | Pyrite | Mixed-layer illite/smectite | Chlorite | Kaolinite |
|---|---|---|---|---|---|---|---|---|---|---|
| Mineral content (%) | I | 31.7 | 4.9 | 2.3 | 3.6 | 2.6 | 3.1 | 38.8 | 9.3 | 3.4 |
| | II | 30.6 | 6.7 | 0 | 0.7 | 1.2 | 4.8 | 44.6 | 7.2 | 3.6 |
| | III | 30.3 | 5.5 | 1.9 | 3.6 | 1.4 | 2.2 | 40.5 | 11.8 | 2.5 |

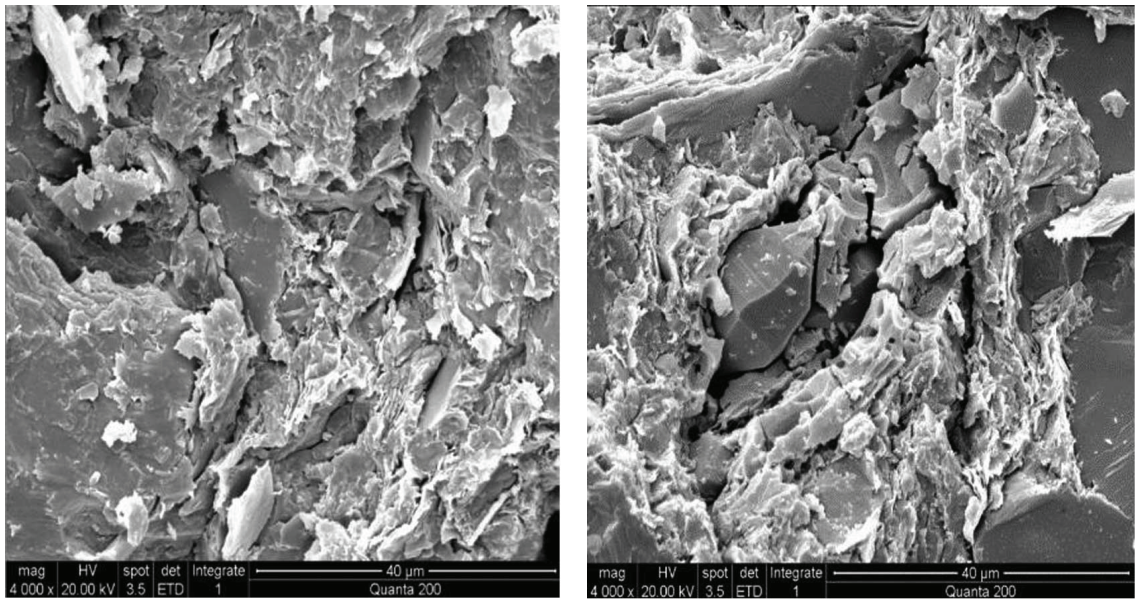


(a) (b)

Figure 6: Core scanning electronic microscope images.

Therefore, the wellbore instability in this area is closely related to the formation characteristics and microstructure of the rock, which is mainly summarized in the following two points: On the one hand, under the action of external forces, the rock of the borehole wall easily breaks along the microfracture or bedding plane. For example, the development of microcracks or tectonic stress concentrations in hard brittle rocks can result in fracturing and spalling of borehole walls and, in turn, wellbore instability. On the other hand, the wall rock is eroded by drilling filtrate and becomes increasingly deep with invasion, while the shale strength and bonding force between the bedding planes decreases with the intensification of hydration and dispersion, which easily produces complicated accidents such as shale cracking, falling blocks, and collapse.

## 3. Mechanism of Borehole Wall Hydration Damage Instability

Shale is usually composed of clay minerals, terrigenous clastic minerals, and autogenous nonclay minerals. Once the shale wall is exposed to the water of the drilling fluid, clay hydration occurs, such as water absorption, swelling, dispersing, and the stress distribution around the borehole wall also changes, causing an increase in pore pressure in the wellbore zone. Meanwhile, the complex chemical action of the drilling fluid on the stratum rock and subsurface fluid softens the shale rock and changes the parameters of the rock mechanics performance, e.g., a strength and binding force reduction between the bedding planes, an elastic modulus reduction, and a Poisson's ratio increase. Therefore, this change is a complex physicochemical process with mechanical and chemical interactions.

Damage mechanics is a mechanical discipline that studies the damage evolution and development until fracture of materials and structures during the deformational process. Its core purpose is studying the process of the damage evolution of media. In fact, the damaged material of rock is anisotropic, and therefore, the damage variable can be measured by tensor and not scalar means. However, for calculation convenience, this study considered the damage to be isotropic and was reduced to one-dimensional problems.

In the study of rock damage mechanics, the damage state is usually described by the variation in rock strength parameters. According to the hypothesis of strain equivalence, the one-dimensional constitutive equation of damaged material [51] can be obtained by the nominal stress of undamaged material in the following form:

$$\varepsilon = \frac{\sigma}{\tilde{E}} = \frac{\tilde{\sigma}}{E} = \frac{\sigma}{E(1-D)}. \tag{2}$$

From equation (2), the effective elastic modulus for the damage material is as follows:

$$\tilde{E} = E(1-D). \tag{3}$$

Therefore, the damage variable expressed by the modulus of elasticity is as follows:

$$D = 1 - \frac{E}{E_0}. \tag{4}$$

Equations (2)–(4) are the starting point of the research on the damage problem.

*3.1. Transfer Function between Drilling Fluid and Shales.* It is assumed that both water molecules and solutes can be transported between the drilling fluid and shales. The interaction between the drilling fluid and the shale, such as the hydraulic pressure, chemical potential, electric potential, and temperature potential differences, is the main driving force of the drilling fluid diffusion and as a result determines the direction, quantity, and velocity of drilling fluid transfer.

*3.1.1. Hydraulic Pressure Difference between the Drilling Fluid and Formation Water.* In conventional balanced drilling, to increase the drilling rate, there is a certain hydraulic pressure difference between the drilling fluid and formation water as follows:

$$\nabla P = P_{df} - P_{sh}. \tag{5}$$

*3.1.2. Chemical Potential Difference between the Drilling Fluid and Formation Water.* During the drilling process of shale formation, the great salinity difference between the drilling fluid and formation water is bound to form a strong chemical potential difference, which drives the drilling fluid to migrate from the wellbore or fracture to the shale matrix. The chemical potential difference [52] is as follows:

$$U_m = \frac{u_{w,df} - u_{w,sh}}{V_w} = 10\left(P_{w,df} - P_{w,sh}\right) + \frac{RT}{V_w} \ln \frac{x_{df}}{x_{sh}}. \tag{6}$$

As shown in equation (6), the chemical potential of the water component in the solution is related not only to the concentration of the solution but also to the pressure. When the salinity difference of the solution is not considered, the driving force is the pressure difference $U_m = P_{w,df} - P_{w,sh}$, that is, the conventional viscous driving force. When the difference in environmental pressure between the formation water and fracturing fluid is considered, the driving force becomes $(RT/V_w) \ln (x_{df}/x_{sh})$, and the driving force of the water migration is reduced to the osmotic pressure.

*3.1.3. Electrochemical Potential Difference between the Drilling Fluid and Shale.* In a shale formation, there is a large amount of clay minerals, such as montmorillonite, chlorite, and kaolinite, and the high valence cations ($Si^{4+}$ and $Al^{3+}$) in clay minerals can be replaced by low-valence cations ($Mg^{2+}$, $Ca^{2+}$, $Na^{+}$, etc.) of the drilling fluids. The charge is out of balance because of the cation exchange in the eight surface wafers and the tetrahedral wafer. To achieve a charge equilibrium, cations must be adsorbed from the

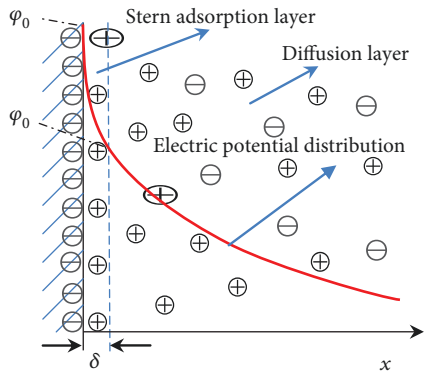


Figure 7: Diffusion double-electron model.

surrounding drilling fluid, also known as compensation ions. According to the theory of double-layer chemistry, a portion of the compensation ions is tightly adsorbed on the surface of the clay slices to form an adsorption layer, and the other parts are concentrated around the clay slices to form a diffusion double-electron layer, as shown in Figure 7.

The concentration of ions in the diffusion layer is a Boltzmann distribution with electric potential [53] as follows:

$$c_{\pm}^{i} = c_{0\pm}^{i} \exp\left(\frac{\mu z_i FU}{RT}\right). \tag{7}$$

It is assumed that salt completely dissociates into positive and negative ions in the solution, both of which are symmetrical salts without ionic association.

$$\begin{aligned} z_{i+} &= z_{i-} = z_i, \\ c_{0+}^{i} &= c_{0-}^{i} = c_0^{i}. \end{aligned} \tag{8}$$

The charge density in the diffusion layer is $\rho_E$.

$$\begin{aligned} \rho_E &= F\sum_i z_i c_{\pm}^{i} = F\sum_i \left\{ c_0^{i} z_i \left[ \exp\left(\frac{-z_i FU}{RT} - \frac{z_i FU}{RT}\right)\right]\right\} \\ &= -2F\sum_i \left[ z_i c_0^{i} \sin h\left(\frac{z_i FU}{RT}\right)\right]. \end{aligned} \tag{9}$$

The following equations are obtained from the Poisson equation $dU/dx = \rho_E/\varepsilon$.

$$\frac{d^2U}{dx^2} = \frac{2F}{\varepsilon}\sum_i \left[ z_i c_0^{i} \sin h\left(\frac{z_i FU}{RT}\right)\right]. \tag{10}$$

The two sides of equation (10) are multiplied by $(dU/dx)^{-1}$ and integrated under a $dU/dx$ boundary condition. The potential equation for the diffusion layer of the clay slices is obtained (11) as follows:

$$U_s = \frac{dU}{dx} = -\left(\frac{8RT}{\varepsilon}\right)^{0.5} \sum_i \left[ z_i c_0^{i} \sin h\left(\frac{z_i FU}{RT}\right)\right] dx. \tag{11}$$

*3.1.4. Temperature Potential Difference between the Drilling Fluid and Shale Formation.* Because the borehole annulus circulating drilling fluid temperature and the formation temperature are not the same, this leads to an obvious change in the wellbore rock moisture content distribution. It has been shown that the moisture content of the cold end increases, the moisture content of the hot end decreases, and the distribution of the moisture content is not uniform and can be approximated to a straight line after a stable change. Thus, the temperature potential difference [54] between the drilling fluid and shale formation can be described as follows:

$$U_T = -a(2 + \rho g)^{b} (\text{grad } T)^{c} + \text{grad } f_w. \tag{12}$$

In summary, there are several driving forces of drilling fluid diffusion. The diffusion of the drilling fluid is related not only to the physical and chemical properties of the drilling fluid but also to the temperature, stress, and physical and chemical properties of the shale formation. During the research process, diffusion coefficients are often used to replace their complex coupling effects.

*3.2. Shale Hydration Diffusion Model.* The mathematical description of the damage evolutionary process of mud shale is derived from the beginning of the hydration. Based on the study of the components, physicochemical properties, and electrochemical characteristics comprehensively applying the theory of diffusion of seepage mechanics, a mathematical model of water absorption and diffusion of the shale wall can be established under hydraulic pressure coupled with the chemical potential difference.

Supposing $q$ is the mass of the moisture diffusion and $f_w(r, t)$ is the water content of the shale from the wellbore axis $r$ at time $t$,

$$\nabla q = \frac{\partial f_w(r, t)}{\partial t}. \tag{13}$$

According to the fluid transfer mechanism between the drilling fluid and shale, the mass of the moisture diffusion is obtained as follows:

$$q = C_f \nabla f_w(r, t). \tag{14}$$

Substituting equation (14) into equation (13), the basic equation of water diffusion of the shale is obtained in the cylindrical coordinate system as follows:

$$C_f \frac{1}{r}\frac{\partial}{\partial r}\left(r\frac{\partial f_w(r, t)}{\partial r}\right) = \frac{\partial f_w(r, t)}{\partial t}. \tag{15}$$

Simplification of equation (15) yields equation (16) as follows:

$$\frac{\partial^2 f_w(r,t)}{\partial r^2} + \frac{1}{r}\frac{\partial f_w(r,t)}{\partial r} = \frac{1}{C_f}\frac{\partial f_w(r,t)}{\partial t}. \tag{16}$$

The boundary conditions and initial conditions are provided by the following formula:

$$\begin{cases} f_w(r_b,t) = f_{bs}, \\ \lim\limits_{r\to+\infty} f(r,t) = f_0, \\ f_w(r,0) = f_0. \end{cases} \tag{17}$$

Solving equations (16) and (17), one can obtain the analytical solution of the water content of shale $f_w(r,t)$ in the formation around the wellbore, as shown in

$$f_w(r,t) = f_0 + (f_{bs} - f_0) \cdot \left[1 + \int_0^a e^{-C_f\cdot\zeta^2\cdot t}\frac{J_0(\zeta r)Y_0(\zeta a) - Y_0(\zeta r)J_0(\zeta a)}{J_0^2(\zeta a) + Y_0^2(\zeta a)}\cdot\frac{d\zeta}{\zeta}\right]. \tag{18}$$

Under the experimental conditions, shale water diffusion only extends along the radial direction and can be regarded as one-dimensional seepage. Therefore, the shale water diffusion equation (16) can be simplified to equation (19) as follows:

$$C_f\frac{d^2 f_w(r,t)}{dx^2} = \frac{df_w(r,t)}{dt}. \tag{19}$$

Combined with the boundary condition and initial condition equation (17), the solution of equation (19) is obtained by the Laplace transform as follows:

$$f_w(x,f) = f_{w0} + (f_{ws} - f_{w0})erfc\left(\frac{x}{2\sqrt{C_f t}}\right). \tag{20}$$

$C_f$ is the water diffusion coefficient of the materials, which is related to the properties of the shale and drilling fluid and can be measured from diffusion experiments.

*3.2.1. Experimental Equipment.* In this experiment, a set of measuring devices was developed by the Southwest Petroleum University of China that could simulate the distribution of the water content of the shale in practice as well as the temperature and pressure conditions. The rock samples collected on site were measured in the laboratory. The experimental equipment was composed of a drilling fluid heating and temperature measuring system, a drilling fluid circulation system, an axial compression system, an oil and water metering system, a computer acquisition system, a confining pressure system, a temperature control system, a safety protection system, and a pressure and resistivity measuring sensor.

*3.2.2. Experimental Method and Steps.* During this experiment, the diffusion coefficient $C_f$ of the shale was measured in the mud drilling fluid (mud prescription: 1% bentonite +0.8% PAV-L+0.2% FT-98+0.05% XCD)+KCl solution, and the content of the KCl solution reached 7%. The debris that retained the original moisture content was placed into a special rock sample box and made into a 25.4 mm × 50 mm standard rock sample over 5 minutes at 5 MPa pressure to serve as the pressure prototype. The specific test process was as follows:

(a) The original water content was first tested. The rock sample was wrapped in an isolation sleeve and placed into a core holder. Then, the drilling fluid (7% KCl solution) was placed into the tank, and the experimental system was checked to ensure that it was in a normal state

(b) At the beginning of the experiment, the confining pressure pump was used to increase the pressure in the high-pressure chamber in the core holder to a confining pressure of 5 MPa, and then, the temperature controller was opened to heat the high-pressure chamber to the reservoir temperature of 80°C. Next, the confining pressure was increased to 15 MPa, and at the same time, the axial pressure was loaded to the planned value of 2.5 MPa. Then, the timing was started

(c) During the course of the experiment, the computer control system was used to maintain the test values as constants

(d) The experiment was divided into four groups with soaking times of 12 h, 24 h, 72 h, and 144 h, respectively. After the test time reached the predetermined value, the temperature control system was gradually removed, and the rock sample was rapidly extracted along the axial direction. The water content was then measured using the dry weight method

Four groups of permeability experiments were conducted on the shale using the 7% KCl solution. The water content for the different axial distances was measured with the resulting data fitted with equation (20) according to the least squares method (Figure 8). It can be seen from Figure 3 that the water content gradually decreased with distance and increased with soaking time, in accordance with the description of equation (11).

*3.3. Mechanical Strength of the Shale Rock.* The hydration softening function of the mud shale is mainly reflected in the change in rock strength. The variation regularity of the shale elastic modulus and rock compressive strength for different water contents and soaking times was investigated using the uniaxial compression experiment method.

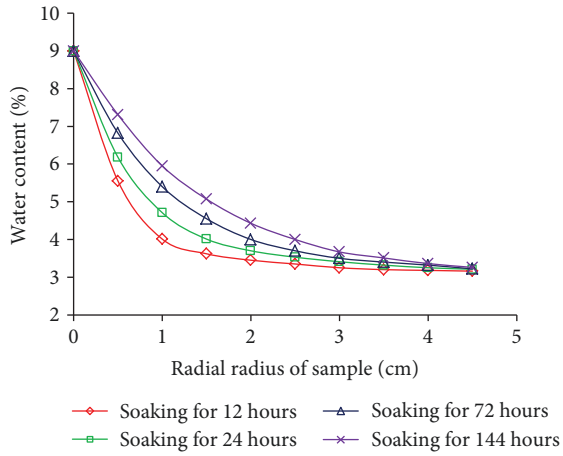


Figure 8: Fitting curve of shale absorbing water in a solution of 7% KCl.

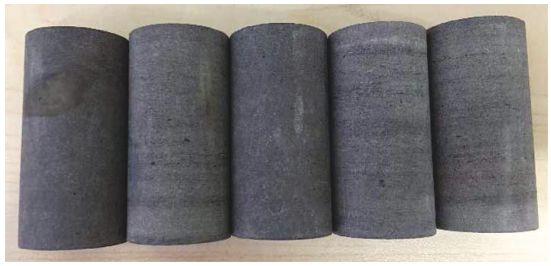

Figure 9: Shale samples.

*3.3.1. Main Instruments.* In accordance with the common petroleum industry standard and guided by the preparation of cores recommended by the International Society of Rock Mechanics (ISRM), the core was processed into a cylindrical standard sample with a diameter of 25 mm and a height of 50 mm (Figure 9); the surface roughness of the end was 0.1 mm. The main equipment used during the uniaxial experiment was an electrohydraulic servo universal testing machine, a static resistance strain gauge, a normal temperature resistance strain gauge, a compensation block, etc.

During this experiment, the resistance strain type load sensor on which 3.0 mm × 5.0 mm resistance strain gauges were mounted was used to measure the stress (Figure 10). The longitudinal and transverse strains of the rock sample were measured by strain gauges parallel and perpendicular to the axis of the cylinder, and the strain gauges were pasted on the central surface of the cylindrical rock sample. A compensating strain gauge was attached to the special piece of rock, which was constructed in a half bridge output to compensate for the effects of pressure and temperature of the work piece and connected to the strain gauge by a signal from the load sensor.

*3.3.2. Experimental Method.* As shown in Figure 11, the electrohydraulic servo universal test machine was used to carry out the uniaxial compression test on the sample. During the experiment, the displacement feedback control system was set at a pressure head speed of 0.01 mm/s, and it recorded the forces needed to produce deformation on site.

Figure 10: Sample to be tested.

*3.3.3. Experimental Results Analysis.* Through experimental data processing, the shale mechanical parameters under different water contents and different times of water absorption were recorded as shown in Figures 12–14.

A shown in Figure 12, the determination of a relationship between the water content and soaking time can be described by three straight lines: $f_w(t) = dt + f'_w$. As shown in Figure 12, $f_w$ increases with $t$ rather rapidly during the beginning segment; then, the rate of increase slows; finally, when immersed for a sufficient time, the shale becomes fully saturated, and the state tends to stabilize with the moisture content unchanged.

Figure 13 shows that during the starting stage, $\sigma_c$ has a large descending slope, and then the slope flattens. When $t$ reaches a certain point, the change in $\sigma_c$ is small, and the curve tends to flatten. Hence, one can see that even if the water content is unchanged, $\sigma_c$ still changes with $t$, but the effect of $t$ gradually decreases.

As shown in Figure 14, similarly, the relationship between the elastic modulus of the shale and the soaking time is approximately divided into three linear relationships with the fitting parameters. During the first stage, it is steeply descending, while during the 2nd stage, it is slowly descending; during the 3rd stage, it is a gentle segment, and the shape is close to the horizon.

The relationship of the uniaxial compressive strength and the modulus of elasticity with water content and soaking time can be established using the aforementioned relations.

Figure 12 shows the relationship between shale water content and soaking time, while Figure 13 shows the relationship between shale strength and soaking time. Figure 14 is actually a combination of Figures 12 and 13, which establishes the relationship between shale strength and water content. As can be seen from Figures 12 and 13, when the rock water content increases from 3.5% to 7%, the drilling fluid filtrate diffuses rapidly to the formation, and the time required is very short (about 70 h). During this time, the drilling fluid

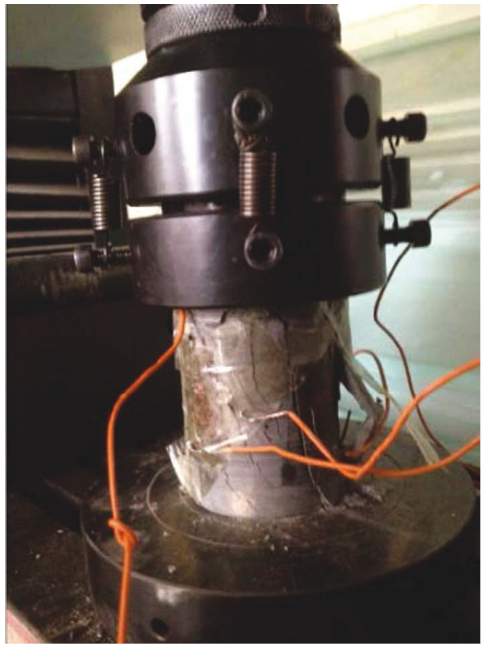

Figure 11: Uniaxial compression test of the rock specimen.

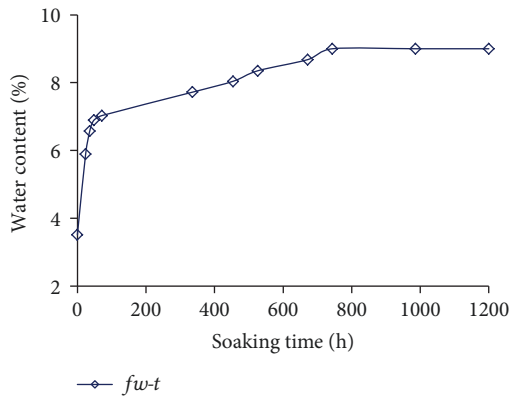


Figure 12: Relationship of water content and soaking time of shale.

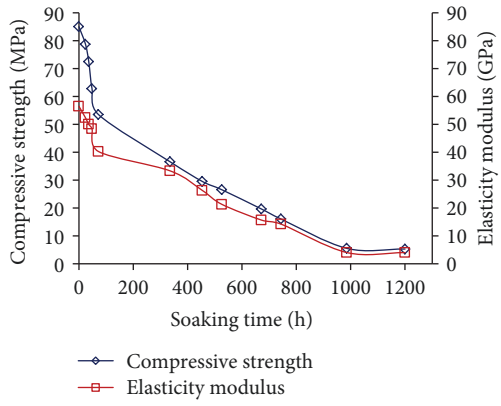


Figure 13: Relationship of uniaxial compressive strength, modulus of elasticity, and soaking time of shale.

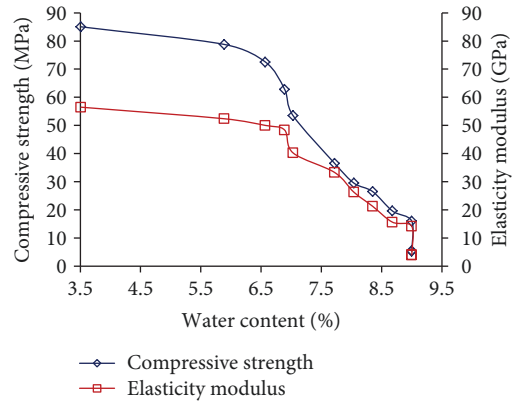


Figure 14: Relationship of uniaxial compressive strength, elastic modulus, and water content of shale.

filtrate mainly flows to the natural fissure or large pores; the water content of the shale thus increases rapidly, causing the shale compressive strength to decrease rapidly. As for Figure 12, the time required for the shale water content to rise from 3.5% to about 6% is very short (about 30 h), the filtrate has not yet diffused into finer pores and fine cracks, the hydration is insufficient, and thus, shale compressive strength changes slowly with the increase of water content, which is also indicated from Figure 14. Figure 14 also shows that it takes a long time for the water content to increase from 6% to 9%, and the filtrate diffusion and hydration time are relatively sufficient, resulting greatly reduced shear strength.

Figure 14 shows the relationship between the uniaxial compressive strength and water content, whose equation is as follows:

$$\sigma_c(f_w) = 0.1568f_w^4 - 4.1675f_w^3 - 37.894f_w^2 + 150.33f_w + 302.03. \quad (21)$$

The relationship between the elastic modulus and water content is as follows:

$$E(f_w) = -9.13f_w + 96.35. \quad (22)$$

*3.3.4. Discussions.* The shale samples are selected from the well section where the wellbore instability problem is more serious. The mineral content of clay is more than 50%, mainly containing mixed-layer illite/smectite (average 41.3%) and chlorite (average 9.4%); from the analysis of compression experiments, the compressive strength and the modulus of elasticity decrease obviously with the soaking time, so the shale has water sensitivity characteristics. Many researchers have also found that shale water sensitivity is closely related to the mineral composition [17, 19, 55], microstructure, and cementation strength of clay particles [19, 31, 34]. Under the driving forces of the hydraulic pressure, chemical potential, electric potential, and temperature potential, the drilling fluid filtrate will enter the shale along the intergranular fractures and microcrack interfaces [19] in the form of diffusion, convection, and penetration, and

hydration will occur. Hydration includes two aspects: hydration expansion and hydration dispersion. The hydration expansion is divided into two stages: a surface hydration stage and a permeation hydration stage. In the surface hydration stage, the clay particles form two layers of water molecules due to adsorption; the surface hydration water absorption speed is fast, and the expansion volume caused by it is approximately 75% to 100%. In the percolation hydration stage, after the two layers of water molecules are adsorbed on the surface of the clay, free water exists in the system, and the compensating cation adsorbed on the surface of the clay leaves the surface of the clay and enters the water to form a diffused electric double layer. The percolation hydration water absorption speed is slowed, and the clay volume is further expanded due to the repulsive action of the electric double layer. Hydration dispersion is also related to mineral types and cementation strength [15, 19, 55]. It can be analyzed from the rock microstructure that water molecules enter the matrix along the intergranular fractures and microcrack interface of the shale, and the mineral particles of the matrix are thus surrounded by water molecules. Thus, on the one hand, the mutual attraction (electrostatic action) and cementation existing between the mineral particles are weakened by the intrusion of water molecules. This is due to the adsorption of water molecules between the mineral particles, which offsets some of the gravitational effects. On the other hand, water molecules and solutes can be transferred between the drilling fluid and shale. After the water molecules and ions enter the shale, they break the original physical and chemical equilibrium, which may cause complex physical and chemical reactions, thus weakening the cementation strength of the cementing material. The mutual attraction between the mineral particles and the weakening of the cementation result in easy separation of the shale matrix, which is prone to cracking and leads to a decrease in strength.

*3.4. Hydration Stress of Shale.* In the shale's original state, all types of forces are balanced. When the shale is hydrated, the entry of water changes the particle concentration in the gap fluid and then affects the repulsive force of the diffused double electron layer and the double electron layer, which destroys the original stress balance. The clay will be adjusted under the action of increasing force $\Delta F$ to achieve a new stress balance, resulting in hydration stress.

The hydration stress [56] is $\sigma_h$, and it is mainly composed of two parts: the diffusion double-electron electrochemical repulsion force and the intermolecular interaction force. From the microstructure model of shale, the total work of all clay minerals in $\delta$ volume is equal to the sum of the work completed by the electric double-layer repulsion force and van der Waals force in the $i$ direction.

$$W_t^i = W^i + W_{cs}^i = \varepsilon_{h_i} \sum_j \left[ h_j \Delta F_j(h_j) n_j \int_0^\pi P_{ja_i} \cos^2 a_i da_i \right] + \varepsilon_{h_i} h_{cS} \Delta F_{cS}(h_{cS}) n_S n_{cS} \int_0^\pi P_{Sa_i} \cos^2 a_i da_i. \tag{23}$$

According to the principle of energy equivalence, because of the hydration in $\delta$ volume, the total work of all clay in the $i$ direction is equal to the hydration stress $\sigma_h$ component, and $\sigma_{hi}$ produces the strain energy.

$$\frac{1}{2}\sigma_{h_i}\varepsilon_{h_i} = \varepsilon_{h_i} \sum_j \left[ h_j \Delta F_j(h_j) n_j \int_0^\pi P_{ja_i} \cos^2 a_i da_i \right] + \varepsilon_{h_i} h_{cS} \Delta F_{cS}(h_{cS}) n_S n_{cS} \int_0^\pi P_{Sa_i} \cos^2 a_i da_i. \tag{24}$$

The shale hydration stress is calculated via equation (24) as follows:

$$\sigma_{h_i} = \begin{cases} 2\left\{ \sum_j \left[ h_j \Delta F_j(h_j) n_j \int_0^\pi P_{ja_i} \cos^2 a_i da_i \right] + h_{cS} \Delta F_{cS}(h_{cS}) n_S n_{cS} \int_0^\pi P_{Sa_i} \cos^2 a_i da_i \right\}, & i = k, \\ 0, & i \neq k. \end{cases} \tag{25}$$

Therefore, hydration stress is another factor causing the collapse instability of the borehole wall and is also known as a mechanical factor. The hydration stress changes the original crustal stress and causes stress redistribution of the surrounding rock of the borehole wall.

*3.5. Determination of Shale Damage Variables in the Water.* The weakening degree of shale strength in water relies on some factors: the physical properties, water content, density, stress state of the rock, and so on. According to the theory of rock strength deformation and failure [57], when the stress deviator of mud shale is less than the rock threshold, the volume strain of the mud shale is elastic. When the stress deviator is greater than the threshold, a dilatation phenomenon will occur in the rock. In this state, the volume strain is the sum of the elastic and dilatation strain, i.e., as follows:

$$\varepsilon_v = \frac{(1-2\mu)}{E_0}\left(\sigma_x + \sigma_y + \sigma_z\right) - 3T_0\left(\frac{\sigma_{oct}}{S}\right)^n. \tag{26}$$

When $\sigma_{oct} > S$, shale expansion occurs.

Combined with the aforementioned experimental results, the compressive strength and elastic modulus of the mud shale are four-power and one-power equations of water

content, respectively. The weakening equation of rock strength and elastic modulus related to dilatation can be obtained as follows:

$$\sigma_c(\sigma_m) = A_1[f_w(\sigma_m)]^4 + A_2[f_w(\sigma_m)]^3 + A_3[f_w(\sigma_m)]^2 + A_4[f_w(\sigma_m)] + \sigma_{c0}, \tag{27}$$

$$E(\sigma_m) = E_0 - Bk_s\rho_w\left[\frac{1}{\rho_0(1+0.01f_{w0})} - \frac{(1-2\mu)\sigma_m}{\rho_0(1+0.01f_{w0})E_0} + \frac{3T_0}{\rho_0(1+0.01f_{w0})}\left(\frac{\sigma_{oct}}{S}\right)^n - \frac{1}{\rho_s}\right], \tag{28}$$

where $\sigma_m = (1/3)(\sigma_x + \sigma_y + \sigma_z)$, and

$$f_w(\sigma_m) = k_s\rho_w\left[\frac{1}{\rho_0(1+0.01f_{w0})} - \frac{(1-2\mu)}{\rho_0(1+0.01f_{w0})E_0} + \frac{3T_0}{\rho_0(1+0.01f_{w0})}\left(\frac{\sigma_{oct}}{S}\right) - \frac{1}{\rho_s}\right] \times 100\%. \tag{29}$$

The relationship of damage variable $D$ with stress state, physical properties, density, etc. can be observed by taking equation (27) into equation (4).

$$D = \frac{B}{E_0}k_s\rho_w\left[\frac{1}{\rho_0(1+0.01f_{w0})} - \frac{3(1-2\mu)\sigma_m}{\rho_0(1+0.01f_{w0})E_0} + \frac{3T_0}{\rho_0(1+0.01f_{w0})}\left(\frac{\sigma_{oct}}{S}\right)^n - \frac{1}{\rho_s}\right] \times 100\%. \tag{30}$$

Equation (30) is the evolutionary equation of the rock water damage variable vs. the stress state, which is closely related to the dilatation.

*3.6. Determination of the Cycle of Shale Borehole Wall Collapse.* The interaction of water and rock that results in the deterioration of rock strength has a strong time dependence. The evolutionary equation of the water damage variable and the previous experiment can be synthetized together to establish the relationship between the damage variable and the soaking time, as well as the fitting relation of the damage variable under different water contents (Table 2).

The fitting formula of the damage function with time can be derived by the experiment as follows:

$$D = -5\times10^{-7}t^2 + 0.0013t + 0.0733\left(R^2 = 0.9873\right). \tag{31}$$

The fitting formula for the damage function with water content can similarly be obtained as follows:

$$D = -0.0036f_w^4(r,t) + 0.0845f_w^3(r,t) - 0.6913f_w^2(r,t) + 2.3951f_w(r,t) - 2.9966\left(R^2 = 0.9994\right). \tag{32}$$

Table 2: Changing relationship of damage variable, soaking time, and water content of shale.

| Group | Soaking time (h) | Water content (%) | Damage variable |
|---|---|---|---|
| 1 | 0 | 3.51 | 0.005 |
| 2 | 24 | 5.59 | 0.071 |
| 3 | 36 | 6.17 | 0.128 |
| 4 | 48 | 6.39 | 0.174 |
| 5 | 72 | 6.63 | 0.231 |
| 6 | 336 | 7.52 | 0.452 |
| 7 | 454 | 7.84 | 0.531 |
| 8 | 526 | 8.15 | 0.594 |
| 9 | 672 | 8.54 | 0.692 |
| 10 | 744 | 9.00 | 0.756 |
| 11 | 986 | 9.00 | 0.901 |
| 12 | 1200 | 9.00 | 0.904 |

It is known from equation (20) that the water content is a function of soaking time and distance from the well axis, and the damage variable function equation (32) time partial derivative is as follows:

$$\frac{\partial D}{\partial t} = -0.0144f_w^3(r,t) + 0.2535f_w^2(r,t) - 1.3826f_w(r,t) + 2.3951. \tag{33}$$

Let $\partial D/\partial t = 0$, when

$$-0.0144f_w^3(r,t) + 0.2535f_w^2(r,t) - 1.3826f_w(r,t) + 2.3951 = 0. \tag{34}$$

Equation (34) is the damage evolutionary limit equation of shale, which can approximate the collapse period of the shale wall.

*3.7. Computational Procedure.* Based on the theory and experiment of shale hydration damage instability, the collapse period of damage instability under different conditions was solved using computer numerical analysis. Figure 15 shows the specific numerical flow chart.

## 4. Practical Example Analysis

Using the previous calculation method of shale hydration damage, the following analyzes the raw data of a well in the mud shale layer of the Fuling Shale Gas Field and calculates the collapse pressure and collapse instability period of the shale layer regarding the stress field of the surrounding rock, modulus of elasticity, and compressive strength as variable parameters. The original parameters of a well in the Fuling Shale Gas Field are as follows: vertical depth $h = 2380$ m, borehole radius $r_w = 10.80$ cm, crustal stress $\sigma_H = 39.5$ MPa, maximum horizontal principal stress $\sigma_1 = 45.2$ MPa, minimum horizontal principal stress $\sigma_3 = 36.8$ MPa, initial cohesive force $\tau_0 = 18.7$ MPa, initial internal friction angle $\theta = 31.58°$, Poisson's ratio $\mu = 0.25$, modulus of elasticity

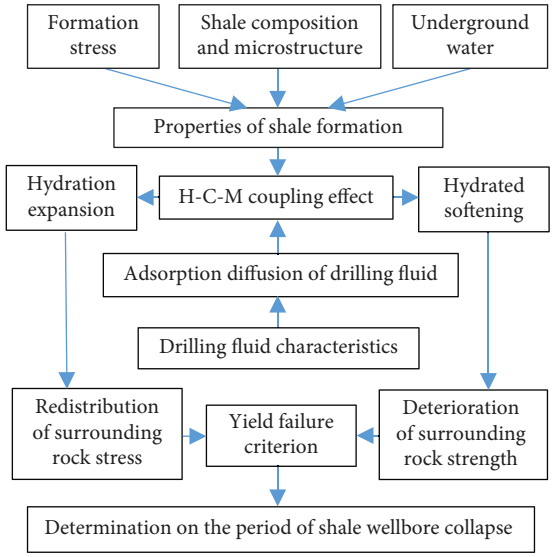


Figure 15: Flowchart of numerical calculation. The H-C-M coupling effect is the hydro-chemo-mechanical coupling effect.

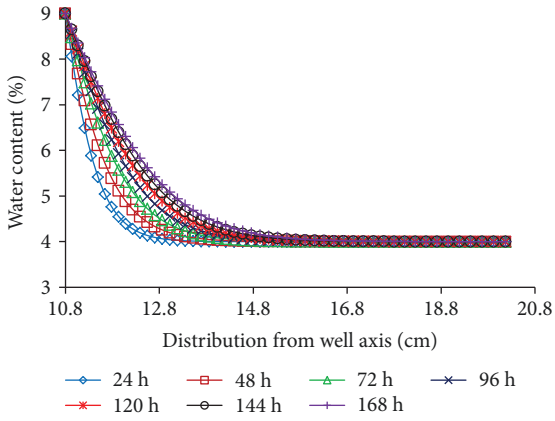


Figure 16: Distribution of water content in the rock wall.

$E = 40\,000$ MPa, diffusion coefficient of water absorption $C_f = 0.0134\,\text{cm}^2/\text{h}$, effective stress coefficient $\alpha = 0.4$, expansion coefficient of water absorption $K_1 = 0.0333$, $K_2 = 0.832$, initial damage value $D_0 = 0.2$, initial water content $f_{w0} = 0.34$, and saturation moisture content $f_{ws} = 9\%$.

*4.1. Distribution Law of Water Content of Borehole Surrounding Rock.* According to the aforementioned parameters and water absorption diffusion in equation (20), the water absorption law of the surrounding rock of a 215.9 mm borehole with time was analyzed, and the relation curves of water content vs. distance from the well axis under different soaking times were obtained (Figure 16).

*4.2. Damage Variable Changes of Borehole Surrounding Rock.* The damage variable changing law with time and space was determined from equation (32) after water absorption of the shale (Figure 17).

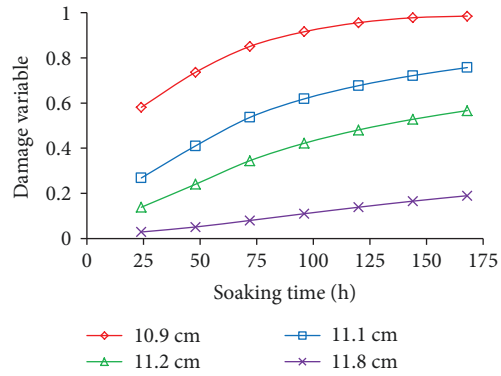


Figure 17: Variation in the damage variable for different depths in the rock wall.

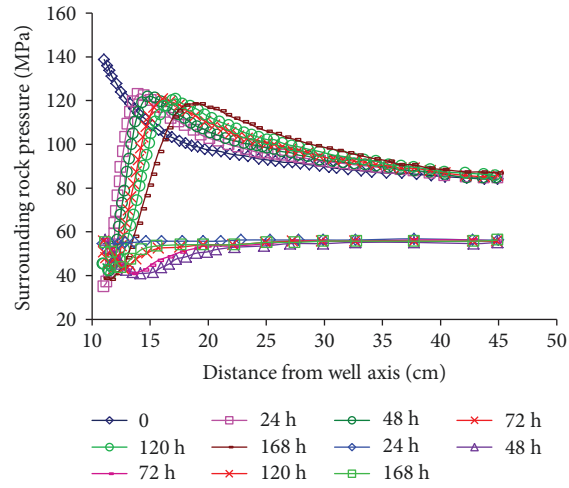


Figure 18: Distribution of the stress field in the rock wall.

It can be seen that the shale damage collapse cycle was 125–175 h (Figure 17). However, the rock strength weakening was not the only reason leading to collapse and failure of the shale borehole; the swelling force caused by water swelling was also an important reason.

*4.3. Distribution Law of the Stress Field of the Borehole Surrounding Rock.* The water swelling of the shale of the borehole wall causes the redistribution of the stress field of the surrounding rock, and the stress distribution law of borehole surrounding rock was obtained by computer solution of this stress field (Figure 18). As shown in Figure 18, the swelling force was generated after shale hydration, which causes stress redistribution of the borehole surrounding rock and allows the tangential stress to reach a maximum at a distance of 2–5 cm from the borehole wall. With time elapsing, the maximum value of this tangential stress varies a little, but its position moves deeper into the strata. As a result, the hydration damage zone of the shaft lining is continuously expanding until the shaft wall shows periodic collapse.

*4.4. Collapse Pressure Changing Law of the Hydration Damage of the Borehole Surrounding Rock.* Using computational

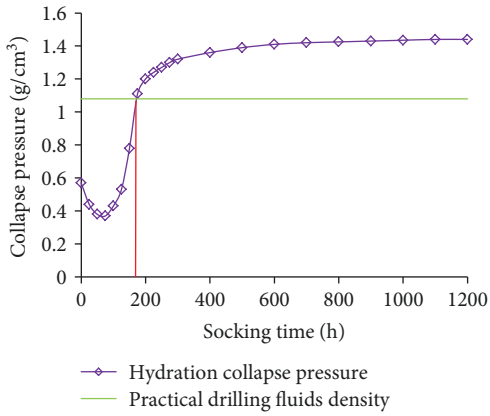


Figure 19: Variation of collapse pressure with soaking time.

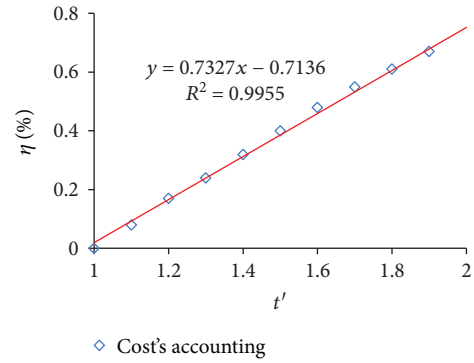


Figure 20: Variation rule between $\eta$ and $t'$.

tools, the change in collapse pressure in the hydration damage with time can be observed in Figure 19, and its hydration collapse cycle can be determined.

From Figure 19, the hydration damage action changes the hydrostatic column pressure required by the shale stability. In contrast, during the early stages of hydration, the collapse pressure coefficient decreases and reaches a minimum in approximately 75 h. After this, the coefficient sharply increases with the hydration time, and after approximately 500 h, it tends to stabilize. From the aforementioned theoretical calculation, the cycle of hydration collapse in the Fuling Shale Gas Field is approximately 168 h (7 days).

The collapse period of deformation can be determined by the collapse pressure curve of the different hydration times. For example, if the used drilling fluid density is 1.08 g/cm$^3$, the collapse cycle can be obtained from a term of approximately 7 days. If the drilling fluid density is 1.41 g/cm$^3$, the collapse cycle is approximately 25 days. Thus, by optimizing the drilling fluid formulation, once can reduce the collapse pressure of the drilling fluid and increase the collapse period.

*4.5. Discussion.* In this paper, based on a soaking experiment, the damage variable is defined by the elastic modulus, and the relationship between shale damage variables and soaking time is established by the mutual transformation of the variables such as the damage variable, elastic modulus, water content, and soaking time. This method is more convenient for determining and predicting the collapse period of the borehole wall and is easy to use in field practice. Some scholars often define damage variables by area [58], wave velocity [22], pores (number, length, area, or volume) [59], and T2 spectrum of nuclear magnetic resonance (NMR) [56] through different test methods. These different methods are based on the purpose of investigation, but the change law of the damage variable is actually consistent. For instance, ultrasonic technology is used to study the damage characteristics of shale and the law of fracture propagation during the uniaxial compression process [22], while the damage variable is defined by the wave velocity. Our experimental results are in agreement with reference [12] on damage change but show more water sensitivity.

It is worth mentioning that this paper simplifies the shale into isotropic measures, ignoring the influence of the shale weak plane structure on the stability of the borehole wall; thus, it is not convenient to predict the crack initiation and propagation law of the borehole wall surrounding rock cracks. In addition, the effects of temperature change were not considered due to experimental conditions, although temperature change in drilling has a significant influence on wellbore wall stability. Next, we will study anisotropic and weak plane structure shale damage instability in a shale borehole wall under high temperature and high pressure conditions with our partners.

*4.6. Evaluation of Drilling Cost.* The drilling cycle is an important factor affecting the drilling cost; thus, it is very important to accurately estimate the wellbore collapse cycle. On the one hand, the cycle can provide technical parameters for the drilling design, and on the other hand, it can effectively reduce the occurrence of wellbore instability and reduce the drilling cost and economic cost. According to the drilling quota cost calculation [49], the economic loss caused by borehole instability can be expressed as follows:

$$\eta = \frac{C_l}{C_T} = \frac{C_{ml} + C_{ll} + C_{ul} + C_{ol}}{C_m + C_l + C_u + C_o + C_d + C_{oe}} \times 100\%. \quad (35)$$

The economic loss rate of drilling is related to the drilling cycle and borehole instability processing time. Figure 20 shows the variation rule between the economic loss rate of borehole wall instability and nondimensional time $t' = (t_c + t_L)/t_c$.

As shown in Figure 20, the economic costs of drilling increase approximately linearly with the increase in borehole instability treatment time; the growth rate is 0.7327, and the fitting correlation coefficient is 0.995.

## 5. Conclusions

(1) An analysis of Chinese shale gas reserves and national policies on shale gas exploitation shows that shale gas will be of critical importance in providing clean natural gas to China. However, compared to the USA, the cost of shale gas extraction and the complex problems encountered in drilling are the key

issues that need to be overcome. Shale wellbore wall instability is a complex problem that often occurs during drilling

(2) In the presence of solid-liquid coexistence, the surrounding rock bears complex mechanical, physical, and chemical interactions, which deteriorate its mechanical strength parameters, and the effective stress of the rock produced by hydration expansion is sharply increased. Therefore, the phase composition of the shale samples, the development of bedding, and microcracks are all internal mechanisms of instability in the shale borehole wall. This study developed a method to determine the collapse period of a shale borehole wall, which was applied to the Fuling Shale Gas Field of China with a result of approximately 7 days, and evaluated the severity of economic loss caused by wellbore wall instability

(3) In view of the geological characteristics of the Fuling Shale Gas Field, it is necessary to rationally deploy a new drilling fluid system to suppress the filtration of drilling fluid into the rock of borehole walls to prolong the collapse period of the surrounding rock and obtain a longer and safer drilling cycle. At the same time, it is more effective to improve the safe drilling period by reasonably improving the safe density of the practical drilling fluid. Thus, accurately determining the collapse period is a safety guarantee for drilling design and construction and is also a technical guarantee of reducing the drilling cost

## Notations

$C_m$: Material cost of normal drilling
$C_l$: Labor costs of normal drilling
$C_u$: Cost of using machinery of normal drilling
$C_o$: Other costs of normal drilling
$C_d$: Drilling cost
$C_{oe}$: Other engineering expenditures
$C_{ml}$: Material cost of wellbore wall instability treatment
$C_{ll}$: Labor costs of wellbore wall instability treatment
$C_{ul}$: Cost of using machinery of wellbore wall instability treatment
$C_{ol}$: Other costs of wellbore wall instability treatment
$c_{0\pm}^{i}$: Ion valence of ionization ion without electric field influence
$C_f$: Water diffusion coefficient of materials
$D$: Damage variable
$E$: Elastic modulus of damaged material
$E_0$: Elasticity modulus of materials without damage
$E_d$: Elasticity modulus of shale in dry time
$erfc(x/2\sqrt{C_f t})$: Error compensation function
$f_w$: Water content
$f_{w0}$: Natural water content of shale
$f_{ws}$: Saturated water content of shale
$F$: Faraday constant
$\Delta F_j$: Increment of hydration force
$\Delta F_{cS}$: Increment of van der Waals force
$g$: Gravitational acceleration
$h_j$: Electric double layer thickness
$J_0(\zeta a)$: The first types of Bessel functions
$k_s$: Saturation coefficient
$t$: Time
$P_{df}$: Drilling fluid pressure
$P_{sh}$: Formation water pressure
$P_{w,df}$: Water pressure in drilling fluid
$P_{w,sh}$: Water pressure in bedrock
$\nabla P$: Hydraulic pressure difference
$Q$: Flow amount
$\sigma_m$: Mean stress
$\sigma_c$: Uniaxial compressive strength
$\sigma_x, \sigma_y, \sigma_z$: Stress component
$\tilde{\sigma}$: Effective stress
$\sigma_{oct}$: Generalized shear stress
$\rho_w$: Water density
$\rho_0$: Drying density
$\rho_s$: Rock particle density
$\mu$: Rock Poisson ratio
$\varepsilon$: Elastic strain
$\varepsilon_v$: Volume strain (positive pressure) (%)
$\varepsilon_h$: Hydration strain
$\nabla$: Gradient operator
$r_w$: Borehole radius
$R$: Boltzmann constant
$T$: Temperature
$U$: Diffusion layer potential
$U_m$: Chemical potential difference
$U_s$: Electrochemical potential difference
$U_T$: Temperature potential difference
$u_{w,\,df}$: Chemical potential in drilling fluid
$u_{w,sh}$: Chemical potential in formation water
$V_w$: Partial molar volume of water
$W_t{}^i$: Total work of all clay minerals
$W^i$: Work done by electric double layer repulsion force
$W_{cs}^i$: Work done by van der Waals force between the electric layers
$x_{df}$: Mole fraction of water molecules in drilling fluid
$x_{sh}$: Molar fraction of water molecules in formation water
$Y_0(\zeta a)$: The second types of Bessel functions
$z_i$: Ionization ion valence of $i$ salt.

## Data Availability

All the data used to support the findings of this study are included within the article.

## Conflicts of Interest

The authors declare no conflicts of interest.

## Acknowledgments

This work was supported by the National Natural Science Foundation of China (Nos. 51604285, 51174162, 51674200, and 51874320), the Science and Technology Innovation Project of the Key Laboratory of Shaanxi Province China (2014SZS15-Z02), the Open Foundation of the Key Laboratory of Failure Mechanism and Safety Control Techniques of Earth-rock Dams of the Ministry of Water Resources (YK916006), and Yan'an University Doctor Research Initiation Funding (YDBK2018-52), which are gratefully acknowledged.

## References

[1] F. Bilgili, E. Koçak, Ü. Bulut, and M. N. Sualp, "How did the US economy react to shale gas production revolution? An advanced time series approach," *Energy*, vol. 116, pp. 963–977, 2016.

[2] G. Yuan, S. Luo, and J. Zheng, "Policies on promoting the development of China's shale gas industry," *Science & Technology Review*, vol. 36, no. 4, pp. 8–11, 2018.

[3] Q. Zhao, D. X. Liu, S. Yang, and D. M. Luo, "China's shale gas policy and the effect for the industry," in *Sustainable Development*, pp. 225–230, Wuhan, April 2016.

[4] B. Lu, S. Ding, and G. Ma, "Status and tendency of engineering technology in shale gas development within Sinopec," in *The 22nd World Petroleum Congress*, Istanbul, 2017.

[5] C. Zou, Z. Yang, J. Cui et al., "Formation mechanism, geological characteristics and development strategy of nonmarine shale oil in China," *Petroleum Exploration and Development*, vol. 40, no. 1, pp. 15–27, 2013.

[6] T. Guo, "Key geological issues and main controls on accumulation and enrichment of Chinese shale gas," *Petroleum Exploration and Development*, vol. 43, no. 3, pp. 349–359, 2016.

[7] N. Wang and Q. Zhao, *China Shale Gas Economic Evaluation Based on Monte Carlo Simulation*, 22nd World Petroleum Congress, 2017.

[8] Y. Zhu, C. Ge, C. Liu, and C. Zheng, *Can China Duplicate US Shale Gas Revolution? Challenges between Shale Gas Resources and Supply in China*, The 21nd World Petroleum Congress, 2014.

[9] C. Jia, M. Zheng, and Y. Zhang, "Unconventional hydrocarbon resources in China and the prospect of exploration and development," *Petroleum Exploration and Development*, vol. 39, no. 2, pp. 139–146, 2012.

[10] C. Yan, J. Deng, and B. Yu, "Wellbore stability in oil and gas drilling with chemical-mechanical coupling," *The Scientific World Journal*, vol. 2013, Article ID 720271, 9 pages, 2013.

[11] G. M. Bol, S. W. Wong, C. J. Davidson, and D. C. Woodland, "Borehole stability in shales," *SPE Drilling & Completion*, vol. 9, no. 2, pp. 87–94, 1994.

[12] H. Roshan and S. S. Rahman, "A fully coupled chemo-poroelastic analysis of pore pressure and stress distribution around a wellbore in water active rocks," *Rock Mechanics and Rock Engineering*, vol. 44, no. 2, pp. 199–210, 2011.

[13] X. Liu, Y. Ding, P. Luo, and L. Liang, "The impact of drilling unloading on wellbore stability of shale formations," *Petroleum drilling techniques*, vol. 46, no. 1, pp. 10–16, 2018.

[14] M. A. Fam and M. B. Dusseault, "Borehole stability in shales: a physico-chemical perspective," in *SPE/ISRM Rock Mechanics in Petroleum Engineering*, Trondheim, Norway, July 1998.

[15] A. Ghassemi, G. Wolfe, A. Diek, and J. C. Roegiers, "A chemo-mechanical model for borehole stability analyses," in *The 37th U.S. Symposium on Rock Mechanics*, Vail, 1999.

[16] L. Cui, Y. Abousleiman, S. Ekbote, J. C. Roegiers, and M. Zaman, "A software for poroelastic analyses of borehole stability," in *Latin American and Caribbean Petroleum Engineering Conference*, Caracas, Venezuela, April 1999.

[17] J. P. Simpson and H. L. Dearing, "Diffusion osmosis-an unrecognized cause of shale instability," in *IADC/SPE Drilling Conference*, New Orleans, Louisiana, February 2000.

[18] S. K. Choi, C. P. Tan, and R. Freij-Ayoub, "A coupled mechanical-thermal-physico-chemical model for the study of time-dependent wellbore stability in shales," *Elsevier Geo-Engineering Book Series*, vol. 2, pp. 581–586, 2004.

[19] C. Yan, J. Deng, Y. Cheng, M. Li, Y. Feng, and X. Li, "Mechanical properties of gas shale during drilling operations," *Rock Mechanics and Rock Engineering*, vol. 50, no. 7, pp. 1753–1765, 2017.

[20] M. Ostadhassan, H. Jabbari, S. Zamiran, A. Osouli, B. Bubach, and B. Oster, "Probabilistic time-dependent thermo-chemo-poroelastic borehole stability analysis in shale formations," in *US Rock Mechanics/Geomechanics Symposium*, San Francisco, 2015.

[21] F. Amann, E. A. Button, K. F. Evans, V. S. Gischig, and M. Blümel, "Experimental study of the brittle behavior of clay shale in rapid unconfined compression," *Rock Mechanics and Rock Engineering*, vol. 44, no. 4, pp. 415–430, 2011.

[22] Y. Chuanliang, D. Jingen, H. Lianbo et al., "Brittle failure of shale under uniaxial compression," *Arabian Journal of Geosciences*, vol. 8, no. 5, pp. 2467–2475, 2015.

[23] Q. Zhang, W. Jia, X. Fan, Y. Liang, and Y. Yang, "A review of the shale wellbore stability mechanism based on mechanical–chemical coupling theories," *Petroleum*, vol. 1, no. 2, pp. 91–96, 2015.

[24] O. M. Nes, J. Stenebråten, and E. Fjær, "Time dependent borehole stability: effect of static vs. dynamic mud weight," in *SPE/IADC Drilling Conference and Exhibition*, London, 2015.

[25] Q. Wang, G. Wang, H. Jiang, P. Wang, and Y. Liu, "Study on shale wellbore stability coupling," *Fault-Block Oil & Gas Field*, vol. 19, pp. 517–521, 2012.

[26] B. Xue, J. Zhang, X. Tang et al., "Characteristics of microscopic pore and gas accumulation on shale in Long Maxi Formation northwest Guizhou," *Acta Petrolei Sinica*, vol. 36, no. 2, pp. 138–149, 2015.

[27] Y. Su and S. Guo, "Qualitative and quantitative characterization of shale microscopic pore characteristics based on image analysis technology," *Advances in Earth Science*, vol. 31, no. 7, pp. 751–763, 2016.

[28] Y. H. Lu, M. Chen, Y. Jin, and G. Q. Zhang, "A mechanical model of borehole stability for weak plane formation under porous flow," *Petroleum Science and Technology*, vol. 30, no. 15, pp. 1629–1638, 2012.

[29] C. Yan, J. Deng, B. Yu et al., "Research on collapsing pressure of gas shale," *Chinese Journal of Rock Mechanics and Engineering*, vol. 32, no. 8, pp. 1595–1602, 2013.

[30] X. Liu, W. Zeng, L. Liang, and M. Lei, "Wellbore stability analysis for horizontal wells in shale formations," *Journal*

*of Natural Gas Science and Engineering*, vol. 31, pp. 1–8, 2016.

[31] V. Dokhani, M. Yu, and B. Bloys, "A wellbore stability model for shale formations: accounting for strength anisotropy and fluid induced instability," *Journal of Natural Gas Science and Engineering*, vol. 32, no. 32, pp. 174–184, 2016.

[32] N. Halakatevakis and A. I. Sofianos, "Correlation of the Hoek–Brown failure criterion for a sparsely jointed rock mass with an extended plane of weakness theory," *International Journal of Rock Mechanics and Mining Sciences*, vol. 47, no. 7, pp. 1166–1179, 2010.

[33] Z. Liu, M. Chen, Y. Jin, X. Yang, Y. Lu, and Q. Xiong, "Calculation model for borehole collapse volume in horizontal openhole in formation with multiple weak planes," *Petroleum Exploration and Development*, vol. 41, no. 1, pp. 113–119, 2014.

[34] T. Ma, P. Chen, Q. Zhang, and J. Zhao, "A novel collapse pressure model with mechanical-chemical coupling in shale gas formations with multi-weakness planes," *Journal of Natural Gas Science and Engineering*, vol. 36, pp. 1151–1177, 2016.

[35] D. Yi, J. Lui, P. Luo, and L. Liang, "Influence of Weak Plane on Wellbore Stability in Shale Formation," *Chinese Journal of Underground Space and Engineering*, vol. 14, no. 4, pp. 1130–1136, 2018.

[36] Y. H. Lu, M. Chen, Y. Jin, W. F. Ge, S. An, and Z. Zhou, "Influence of Porous Flow on Wellbore Stability for an Inclined Well With Weak Plane Formation," *Petroleum Science and Technology*, vol. 31, no. 6, pp. 616–624, 2013.

[37] T. Ma, C. Yang, P. Chen, X. Wang, and Y. Guo, "On the damage constitutive model for hydrated shale using CT scanning technology," *Journal of Natural Gas Science and Engineering*, vol. 28, pp. 204–214, 2016.

[38] Z. Cui and W. Han, "In situ scanning electron microscope (SEM) observations of damage and crack growth of shale," *Microscopy and Microanalysis*, vol. 24, no. 02, pp. 107–115, 2018.

[39] P. Wang and Z. Qu, "NMR technology based hydration damage evolution of hard brittle shale," *Rock and Soil Mechanics*, vol. 36, no. 3, pp. 687–693, 2015.

[40] J. Chen, "Study and application of anti-sloughing drilling fluid containing nano-micro plugging material," *Oilfield Chemistry*, vol. 34, no. 3, pp. 402–407, 2017.

[41] R. Gholami, H. Elochukwu, N. Fakhari, and M. Sarmadivaleh, "A review on borehole instability in active shale formations: interactions, mechanisms and inhibitors," *Earth-Science Reviews*, vol. 177, pp. 2–13, 2018.

[42] J. Abdo and M. D. Haneef, "Clay nanoparticles modified drilling fluids for drilling of deep hydrocarbon wells," *Applied Clay Science*, vol. 86, pp. 76–82, 2013.

[43] R. Rafati, S. R. Smith, A. Sharifi Haddad, R. Novara, and H. Hamidi, "Effect of nanoparticles on the modifications of drilling fluids properties: a review of recent advances," *Journal of Petroleum Science and Engineering*, vol. 161, pp. 61–76, 2018.

[44] J. G. Xu, Z. Qiu, X. Zhao, and W. Huang, "Hydrophobic modified polymer based silica nanocomposite for improving shale stability in water-based drilling fluids," *Journal of Petroleum Science and Engineering*, vol. 153, pp. 325–330, 2017.

[45] R. Gelet, B. Loret, and N. Khalili, "Borehole stability analysis in a thermoporoelastic dual-porosity medium," *International Journal of Rock Mechanics and Mining Sciences*, vol. 50, pp. 65–76, 2012.

[46] C. Yan, J. Deng, B. Yu et al., "Borehole stability in high-temperature formations," *Rock Mechanics and Rock Engineering*, vol. 47, no. 6, pp. 2199–2209, 2014.

[47] M. Gomar, I. Goodarznia, and S. R. Shadizadeh, "A transient fully coupled thermo-poroelastic finite element analysis of wellbore stability," *Arabian Journal of Geosciences*, vol. 8, no. 6, pp. 3855–3865, 2015.

[48] X. Guo, H. Du, Z. Wei, Y. Li, X. Wei, and S. E. Company, "Discovery and exploration of fuling shale gas field," *China Petroleum Exploration*, vol. 21, pp. 24–37, 2016.

[49] W. Chao, Y. Zang, D. Zhang, and J. Wu, "A method of borehole stability prediction while drilling directional wells and its application," *Acta Petrolei Sinica*, vol. 36, no. 10, pp. 1290–1298, 2015.

[50] X. Jin, S. N. Shah, J. C. Roegiers, and B. Zhang, "Fracability evaluation in shale reservoirs - an integrated petrophysics and geomechanics approach," *SPE Journal*, vol. 20, no. 3, pp. 518–526, 2014.

[51] J. Lemaitre, *A Course on Damage Mechanics*, Spriner, 1992.

[52] F. Wang and Z. Pan, "Numerical simulation of chemical potential dominated fracturing fluid flowback in hydraulically fractured shale gas reservoirs," *Petroleum Exploration and Development*, vol. 43, no. 6, pp. 1060–1066, 2016.

[53] P. Zhang, C. Zuo, D. Zhou, H. Chen, and Y. Liu, *Numerical Simulation on Electroosmotic Flow in a Rectangular Microchannel*, International Conference on Electronic Packaging Technology, 2006.

[54] T. Wang, N. Li, and D. Xie, "Gravitational potential, matrix suction and thermal potential of unsaturated loess soil," *Chinese Journal of Geotechnical Engineering*, vol. 26, no. 5, pp. 715–718, 2004.

[55] J. Sun, J. Liu, L. Yan, and Y. Liu, "Status quo of water base drilling fluid technology for shale gas drilling in China and abroad and its developing trend in China," *Drilling Fluid & Completion Fluid*, vol. 33, no. 5, pp. 1–8, 2016.

[56] Z. Qu and P. Wang, *Mechanics Research on Creep Buckling of the Shale Hydration Damage*, China Science Press, 2016.

[57] Z. Zhu, F. Xing, S. Wang, and W. Xu, "Analysis on strength softening of argillite under ground water by damage mechanics," *Chinese Journal of Rock Mechanics & Engineering*, vol. 23, Supplement 2, pp. 4739–4743, 2004.

[58] D. Krajcinovic, "Damage mechanics," *Mechanics of Materials*, vol. 8, no. 2-3, pp. 117–197, 1989.

[59] T. Ma and P. Chen, "Study of meso-damage characteristics of shale hydration based on CT scanning technology," *Petroleum Exploration and Development*, vol. 41, no. 2, pp. 249–256, 2014.